The University of Chicago

Application of Flood Filling Networks in Evolutionary Neuroscience: Robust Quantitative Analysis of Ommatidia in *Lepidoptera*

A Thesis Submitted for the degree of Bachelor of Sciences with Honors in Neuroscience

The College, The University of Chicago

By

Griffin Shaw Badalamente

Faculty Advisor: Narayanan Kasthuri, Ph.D.

Chicago, IL

May 01, 2021

Abstract

Detailed comparisons of neuroanatomy across different species is an unmet goal in evolutionary neuroscience due to limitations in the rate at which high resolution volumetric datasets can be acquired and analyzed. To overcome this challenge, I combine high-throughput imaging with a flood-filling network (FFN) computer vision algorithm (Januszewski, et al., 2018) for automated image segmentation and reconstruction. FFN shows promise in being able to automate the process of image segmentation by using machine learning, requiring a relatively small ground truth, and showing high accuracy and recall rates. Specifically, I analyzed data collected at Argonne National Laboratory's synchrotron source micro-x-ray computed tomography (μXCT), which possesses imaging rates of about 15 min/mm^3 at a resolution of 600 nm^3, to quickly acquire volumetric datasets of ommatidia structures in several species of *Lepidoptera*. I created a data analysis pipeline allowing for detailed comparison between full eye samples across moths, butterflies, and skippers focusing on evolutionary adaptations based on their typical active periods: diurnal, nocturnal, or crepuscular (following the logic of Barlow, 1952). This pipeline is generalizable to similar anatomical data from other species with compound eyes, and this paper uses it to arrive at some rudimentary biological conclusions pertaining to the evolutionary specializations of the eyes of *Lepidoptera* that exhibit diurnal, nocturnal, and crepuscular behavior. The pipeline is publicly accessible in in a github repository: griffbad/Ommatidia_Pipeline.

Intro

Evolutionary neuroanatomy currently lags other evolutionary fields (such as evolutionary genetics) in the use of novel computational techniques. Modern technology has enabled extremely rigorous and complex analyses of high volumes of data, and neuroanatomy has had a difficult time collecting and digitizing volumetric data at the scale that enables evolutionary conclusions.

As a starting point, the community has turned towards serial electron microscopy (SEM) to acquire a series of two dimensional images that can be stacked and aligned to produce a digitized, high resolution, three dimensional volume of a piece of tissue (Kasthuri, Hayworth, Lichtman, Erdman, & Ackerley, 2007). Serial EM's advantage lies in its high resolution, enabling scientists to resolve synapses, and thus circuits, in the brain. For analysis of gross evolutionary structures where many samples span phylogenies, however, EM is prohibitively slow. Biological structures across species and families can likely be resolved with faster, more scalable techniques with a lower resolution.

One such lower resolution techniques is synchrotron X-ray microtomography (µXCT). Aside from much higher speeds than EM, µXCT also enables non-species specific protocols (i.e. there is no need for molecular tools such as antibodies). Further, microtomography utilizes osmium as the staining agent, which labels all membranes. This allows for non-biased data collection; µXCT gives data on all biological structures from a sample, allowing for exploration of biological space that does not rely on a pre-conceived hypothesis.

Collecting specific data within this large biological space is non-trivial. Traditionally, such volumetric data is collected manually, where a researcher will label and annotate each example of an object in question from a large volume (a process known as segmentation). This is typically done using a software such as Knossos (Boergens K. M., et al., 2017) or Vaa3d (Peng, Ruan, Long, Simpson, & Myers, 2010).

Manual segmentation, however, comes with a host of common problems, amongst which time is the primary issue. Recent estimates put time to fully manually segment a 93x93x60 µm^3 volume at 200,00 – 500,000 hours (Berning, Boergens, & Helmstaedter, 2015). As a result, several segmentation algorithms have been produced to help automate this process. Many of these solutions, however, require either extensive human proofreading or have exceedingly high error rates (Januszewski, et al., 2018). Recently, several novel machine learning algorithms have implemented convolution neural nets (CNNs) to improve the underlying computer vision techniques used for segmentation (MacDonald et al., 2020; Soltanian-Zadeh, Sahingur, Blau, Gong, & Farsiu, 2019; Urakubo, Bullmann, Kubota, Oba, & Ishii, 2019; Helmstaedter M. , et al., 2013). My paper uses a novel technique produced by Michał Januszewski and his team at Google called a Flood Filling Network (FFN) (Januszewski, et al., 2018). FFN embellishes typical CNNs by starting

with an edge detection algorithm to identify discrete objects which it compares to the dataset it was trained with (this dataset is known as the ground truth) (Fig. 1c). This algorithm has been
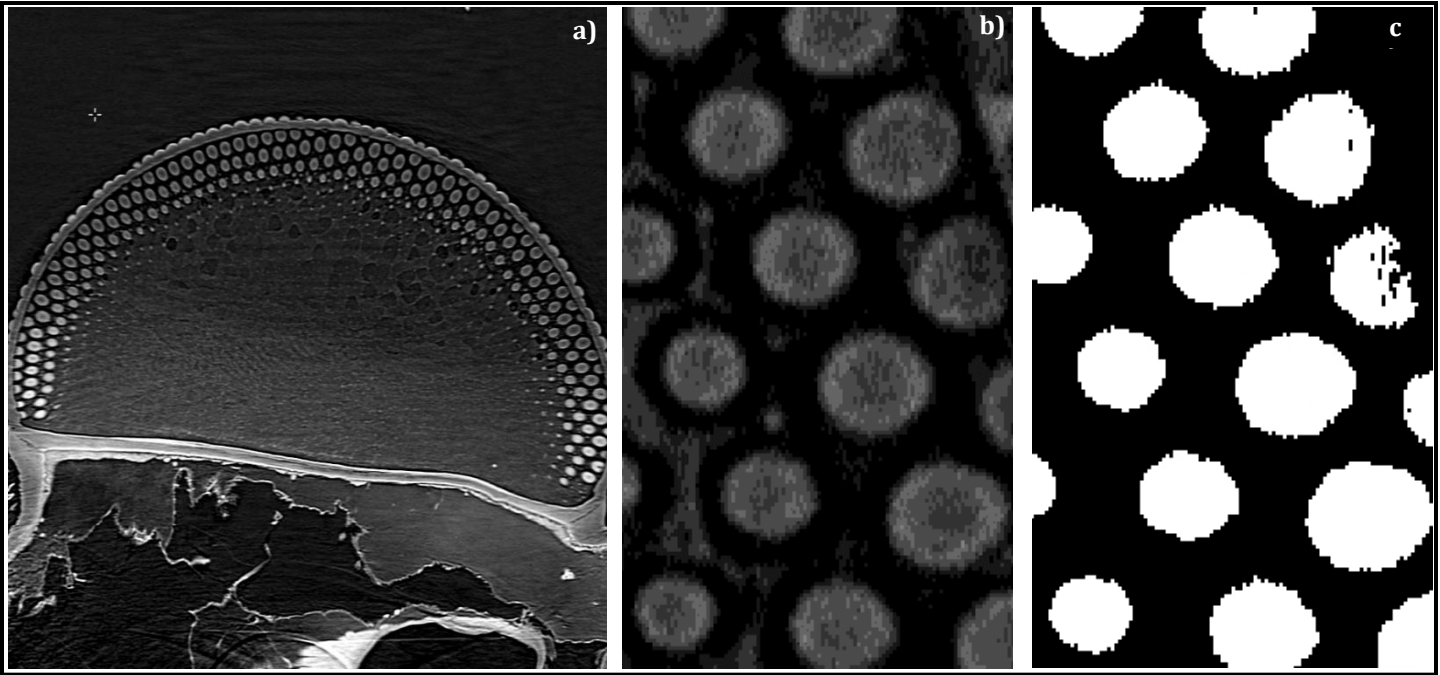
(suborder *Heterocera*) is their divergent activity periods: moths are typically nocturnal, butterflies typically diurnal, and skippers crepuscular. This paper utilizes three dimensional computational

Fig. 1: *Example of data and ground truth. **a)** Full, two-dimensional slice from a three-dimensional volume of a* Lepidoptera *eye, obtained as described via x-ray microtomography. **b)** Zoomed in image focusing on a small number of cones. **c)** Example of ground truth, where the ommatidia are labeled distinctly from the background.*

previously shown to outperform most other automated segmentation algorithms in certain datasets (Linsley, Junkyung, Berson, & Serre, 2020).

This paper applies FFN as a tool to bridge the problems of manual segmentation and applies it in a novel analysis of ommatidial anatomy in insect vision. Specifically, I utilize volumetric data of crystalline cones from ommatidia acquired via FFN from partial and complete eye volumes of moths, butterflies, and skippers (all order *Lepidoptera*) to reach rudimentary conclusions about ommatidial development in similar model specimens. The main evolutionary distinction between butterflies (suborder *Rhopalocera*), skippers (family *Hesperiidae*), and moths

techniques to compare quantitative properties, both global and local, of ommatidia between specimens with distinct behaviors (Table 1). Much of the analysis is based on the landmark work done by H. B. Barlow concerning the limitations imposed by physics on the maximum resolutional capabilities of compound eyes (Barlow, 1952). The quantitative comparisons between behavioral categories is used to inform evolutionary conclusions.

Family	General *Lepidoptera* Type	Behavior
Hesperiidae	Skipper	Crepuscular
Hesperiidae	Skipper	Crepuscular
Nymphalidae	Butterfly	Diurnal
Nymphalidae	Butterfly	Diurnal
Bombycidae	Moth	Nocturnal
Bombycidae	Moth	Nocturnal

Table 1: *Family and behavior of the six specimens used.*

Methods

Collecting the morphologic and volumetric data of digitized crystalline cones involved two main categories of steps: manual work and automated work. The first subsection will focus on the manual work, which involved collecting, preparing, and digitizing the eyes, as well as creating the ground truth for the neural net and, later, cleaning the final data for final analysis. A second subsection will describe the automated work done by the neural net, which accounted for years of manual labor without automation, giving us hundreds of gigabytes of volumetric data. A final subsection will focus on the analysis done to the completed collections of data, explaining the data pipeline that was created.

Fig. 2: a) Diagram of synchrotron X-ray microtomography of a millimeter-scale brain sample (Dyer, et al., 2017). b) Three dimensional rendering of an eye volume from a nocturnal specimen obtained via the methods described.

Manual Work

The first steps – collecting and fixing specimens – were done with the goal of digitizing samples via synchrotron X-ray microtomography (μXCT), which the lab's access to Argonne National Laboratory's μXCT enabled (Fig. 2). This microscopy strategy collects data at an unmatched rate, up to fifteen minutes per one cubic millimeter, but sacrifices some maximum resolution. However, ommatidia are relatively large, so this trade off enables us to digitize the entire eye at a high clip without losing 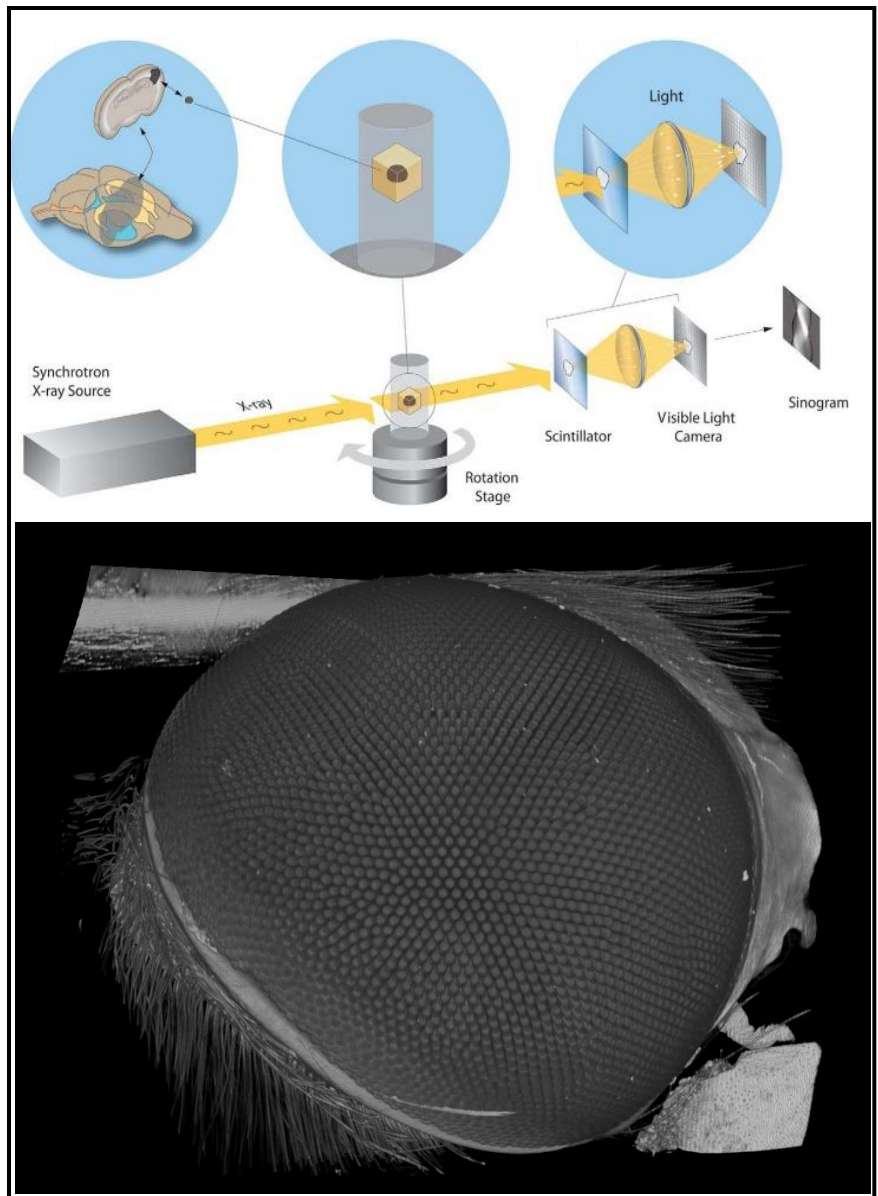information. The lower resolution also means that the size of a fully digitized volume will be on the order of tens, instead of hundreds, of gigabytes. Further, this method is preferable to other volumetric microscopy methods, which involve physically cutting large blocks of resin-bound tissue into nanometer thick slices and treating each slice as a two dimensional image to be stacked together digitally into a 3D volume. Slicing methods come with a whole host of stitching and alignment issues that decrease efficacy and veracity of the data.

The preparation and staining is tested and simple. First, the specimens are anesthetized by placing them at 4°C for ten minutes. Then, while submerged in cold 0.1M HEPES buffer (pH 7.50), their heads are decapitated with scissors, and the eyes are cut off from the head and stained for electron microscopy. For the staining procedure (from Hua, Laserstein, & Helmstaedter, 2015), eyes were washed extensively in cacodylate buffer at room temperature and stained sequentially with 2% osmium tetroxide (EMS) in cacodylate buffer, 2.5% potassium ferrocyanide (Sigma-Aldrich), thiocarbohydrazide, unbuffered 2% osmium tetroxide, 1% uranyl acetate, and 0.66% Aspartic acid buffered Lead (II) Nitrate with extensive rinses between each step (with the exception of the potassium ferrocyanide step). The sections were then dehydrated in ethanol and propylene oxide and infiltrated with 812 Epon resin. The resin-infiltrated tissue was cured at 60°C for three days. This results in a cured resin block that the eyes are set in, which were then sent to Argonne National Laboratory to be digitized via the ID32 beamline at the Advanced Photon Source (APS).

For data collection, the same protocol as Dyer, et al., 2017 was used, the only change being that the 10x objective was used to achieve a resolution of 600 nm^3 per voxel (some samples used a 5x objective to achieve a resolution of 1200 nm^3). Briefly, an exposure time of 0.1 s per projection and 3000 projections at 30 keV was used. The ID32 beamline used a 10 μm thick LuAG:Ce scintillator to convert propagation enhanced X-ray wave into visible light. A microscope objective magnified this signal onto a visible light-scientific CMOS camera (pco.edge 5.5 camera, 3418 × 3418 pixels). A similar digital reconstruction method was used, including the Data Exchange schema developed for synchrotron data (De Carlo, et al., 2014) to collect the volumes as large image stacks that were formatted into an HDF volume using Fiji (Schindelin, et al., 2012).[1]

Automated Work and Finishing Steps

The automated work was mainly an implementation of the Flood Filling Networks neural net algorithm produced by Google (Januszewski, et al., 2018). FFN was developed for reconstruction of neurons, but the highly stereotyped morphology of crystalline cones makes them an ideal candidate for testing FFN application to other areas of neuroanatomy.

For the initial ground truth, I cropped a 70x273x153 pixel (= 42x163x92 μm^3) volume from an arbitrary specimen with easily identifiable ommatidia and filled in the twelve crystalline cones that were completely within the volume. An FFN model trained on this small dataset produced ungeneralizable results – it was able to fill in ommatidia that looked very similar to the ones trained on it but failed on specimens that had significantly distinct ommatidia. To solve

---

[1] Most of the work in collecting volumes was completed before I joined the project.

this, I took results from this first neural net, cropped a larger volume (110x220x175 pixel = 66x132x105 μm³), and filled in the 32 full crystalline cones in that volume (a small portion of this is shown in Fig 1b-c). Training on this volume produced a much more satisfactory neural net, one that produced generalizable results on both the original specimen as well as other species. All manual reconstructions were

breaking volumes into equal section, inferencing them each separately, and stitching their results back together.

Once the data were collected via FFN, there were some slight (and expected) errors in many of the reconstructions. Various stray annotations were cleaned, and outliers were removed using a multi-step cleaning algorithm (Fig. 3). First, objects that were obviously too
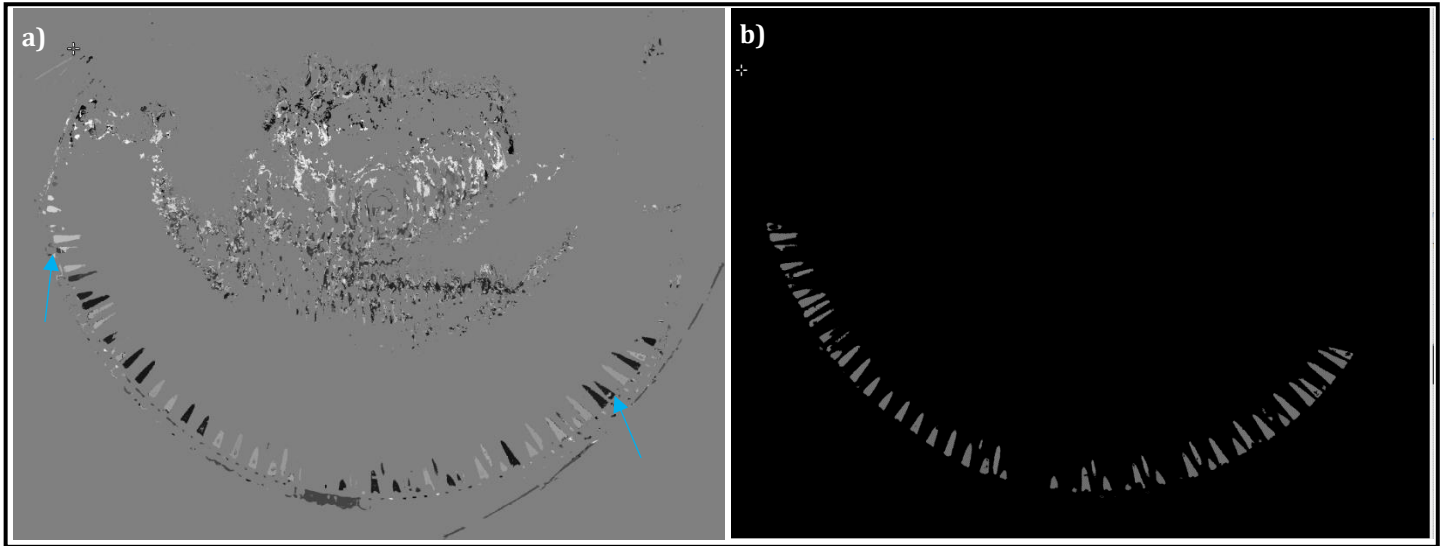

*Fig. 3: Sample results of cleaning scripts. **a)** Raw image directly out of FFN. Blue arrows point to split errors (these errors can be far more common in other datasets). **b)** The same image after cleaning scripts were applied.*

done in Knossos (Helmstaedter, Briggman, & Denk, 2011) and webKnossos (Boergens K. M., et al., 2017).

The goal was to create one neural net that could be used across eye volumes from multiple *Lepidoptera* species and families and would accurately inference ommatidia (using a neural net to segment data is a process known as 'inferencing'). This was achieved with the neural net on the larger volume, and I was able to use this second model to collect data on other full eye volumes. One issue was encountered when Fiji was unable to make HDFs of a full retinal volume due to their large size, which was solved by

large or too small were removed from the dataset. These size thresholds differed per eye but setting a maximum threshold of 1.5x the size of the median object and a minimum threshold of 0.5x that size was a good rule of thumb. This worked because most of the objects from the inference were crystalline cones, and these cones are quite consistent in size. Another error common to FFN is a high rate of split errors, which occur when one object is incorrectly labeled as two different objects (Fig. 3a). To overcome this, my cleaning algorithm converted the label to binary and then relabeled each distinct component. This ensured

that connected voxels that were previously labeled distinctly were uniformly labeled.

Analysis

The direction taken in the creation of the analysis pipeline was heavily informed by H. B. Barlow's landmark paper on the physics that constrain mathematically optimal ommatidia design in insects (Barlow, 1952). His paper establishes a ratio (referred to here as the Barlow Ratio) between the angle of maximum visual resolution per ommatidial cone (φ, calculated with the Rayleigh criterion) and the angle between two neighboring ommatidia (θ) (Fig. 4).

The Rayleigh criterion establishes the angle of maximum resolution at a wavelength of light for a microscope with a given diameter lens. This is a simplification that treats each ommatidium as a microscope where the base of the cone is equivalent to the lens, so the diameter of the base of the cones had to be found. To do so, I applied principle component analysis (PCA) to find the axis of maximum variance in the three dimensional structure of each ommatidium. I first found the centroid of the shape of each ommatidium and then found the top three PCA axes (Fig. 5a). The first principle component axis from the center is equivalent to the axis going from the center of the base of the cone to the tip of the cone. By flattening the three dimensional volume along that axis, I create a two dimensional base of the ommatidium (Fig. 5b). This base is not a perfect circle, but I implement a heuristic based on the fraction of points on a circle that are on the

circumference. Doing so allows us to establish a diameter of each cone, which allows us to establish φ via the Rayleigh criterion.

To find θ, I used the nearest neighbor algorithm implemented in scikit-learn for Python (Predegosa, et al., 2011). By finding pairs of nearest ommatidia (based on their centroids) within the full eye volume, I was able to determine the angle between these two ommatidia by determining the angle between the first PCA axis for each ommatidium. The calculation of φ over θ gives us the Barlow Ratio.

The pipeline also creates a 'platonic' cone for each full volume given. This is done by rotating each individual cone into the same plane by rotating each volume such that all three calculated PCA axes face the same direction for
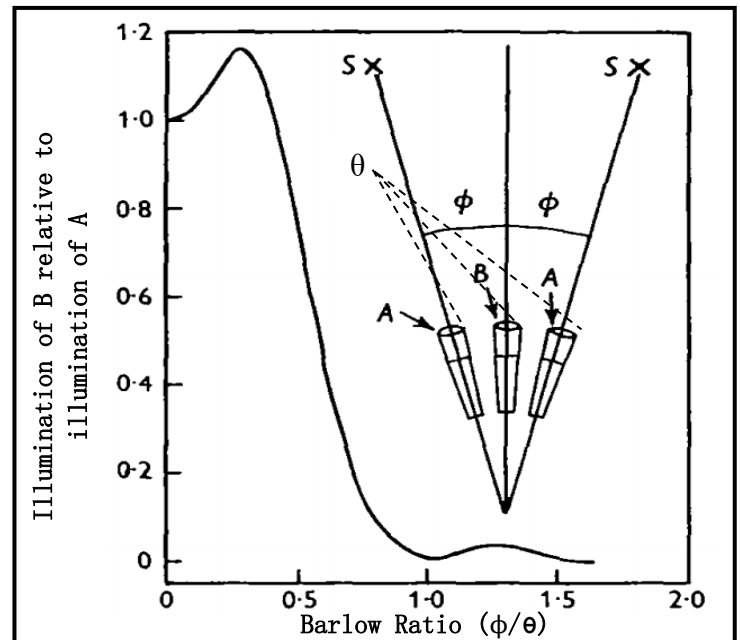

Fig. 4*: Graph of Barlow Ratio. θ is the angle of maximum resolution defined by the Rayleigh criterion. Axes labels and θ indicator added by author, the rest of the image is from Barlow, 1952. A and B refer to hypothetical ommatidia which are treated as microscopes set at angle φ relative to each other. The goal is to minimize the illumination of B ommatidium when A ommatidia are both illuminated by light coming from illumination points SX. This would allow a compound eye to discriminate between the two light sources properly.*

each cone. Once similarly rotated, the data can be overlayed to create a three dimensional heatmap of how often a point occurs amongst the entire population of crystalline cones per sample. This heatmap can be scaled to find a set of points that occur within a certain percent of the population of crystalline cones and construct a three dimensional volume out of it (Fig. 6). This

'platonic' cone can be compared across species and specimens using traditional volumetric comparison methods.

This pipeline is generalizable to similar ommatidial volumetric information from other insect species, enabling extensive comparison across taxonomies and behaviors.
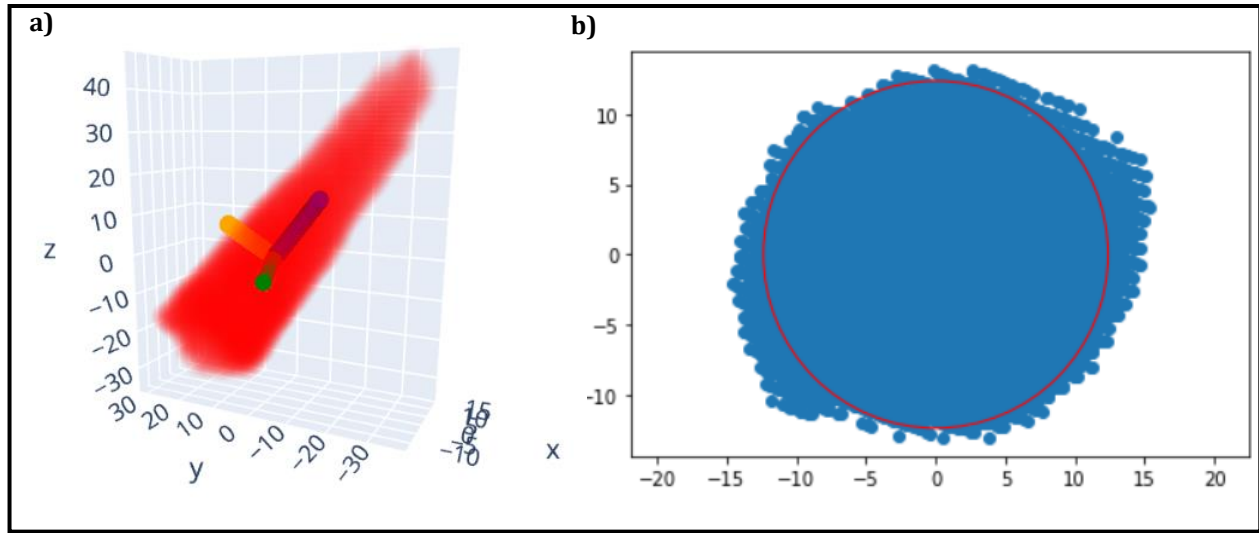

*Fig. 6: Example of PCA process used to characterize and manipulate ommatidia. **a)** An arbitrary cone with its top three PCA results (blue, orange, green, respectively). Note that the centroid of the ommatidia was set to (0,0,0). **b)** Example ommatidia flattened along first PCA to determine diameter. Red circle shows the representative circle that was used to calculate diameter. Units are all in voxels (where each voxel is 600 nm³ for this specimen).*
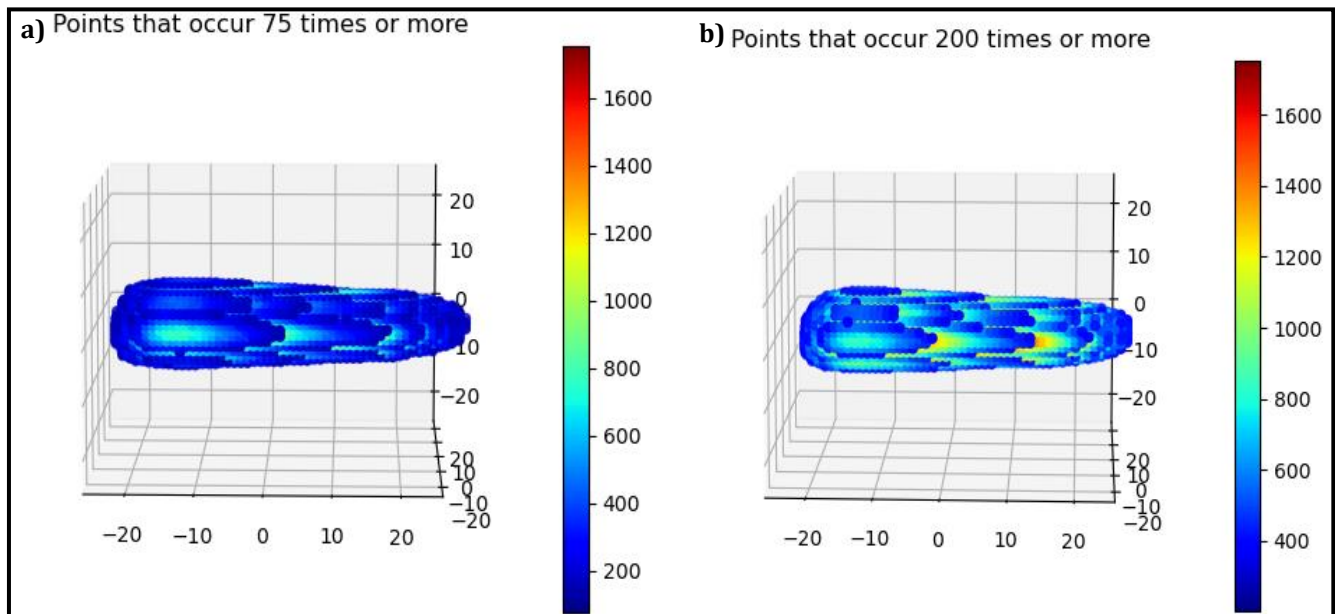

*Fig. 5: 'Platonic' representation of ommatidia from arbitrary sample. There is significant deviation in ommatidium shape between specimens. **a)** Every point that occurred in 75 or more of the ommatidia population. **b)** Every point that occurred in 200 or more of the ommatidia population. All units are in voxels (where each voxel is equivalent to 600 nm³ in this specimen). Voxel colors correspond to the heat bar on the right of each figure, which represent how many crystalline cones contain that point once rotated into the same axis.*
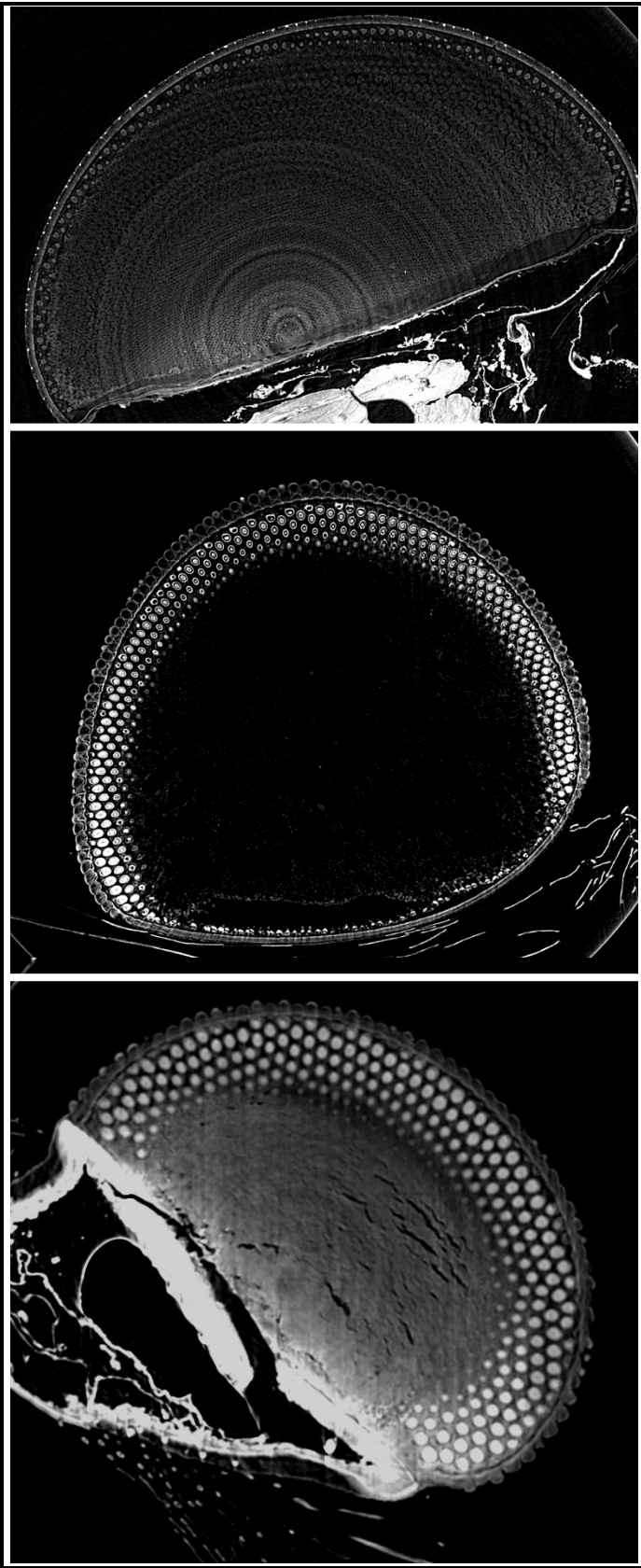
*Fig. 7: Images of three very different cone appearances that were segmented by FFN and included in this paper. **Top** is a diurnal butterfly, **Middle** is a crepuscular skipper, and **Bottom** is a nocturnal moth.*
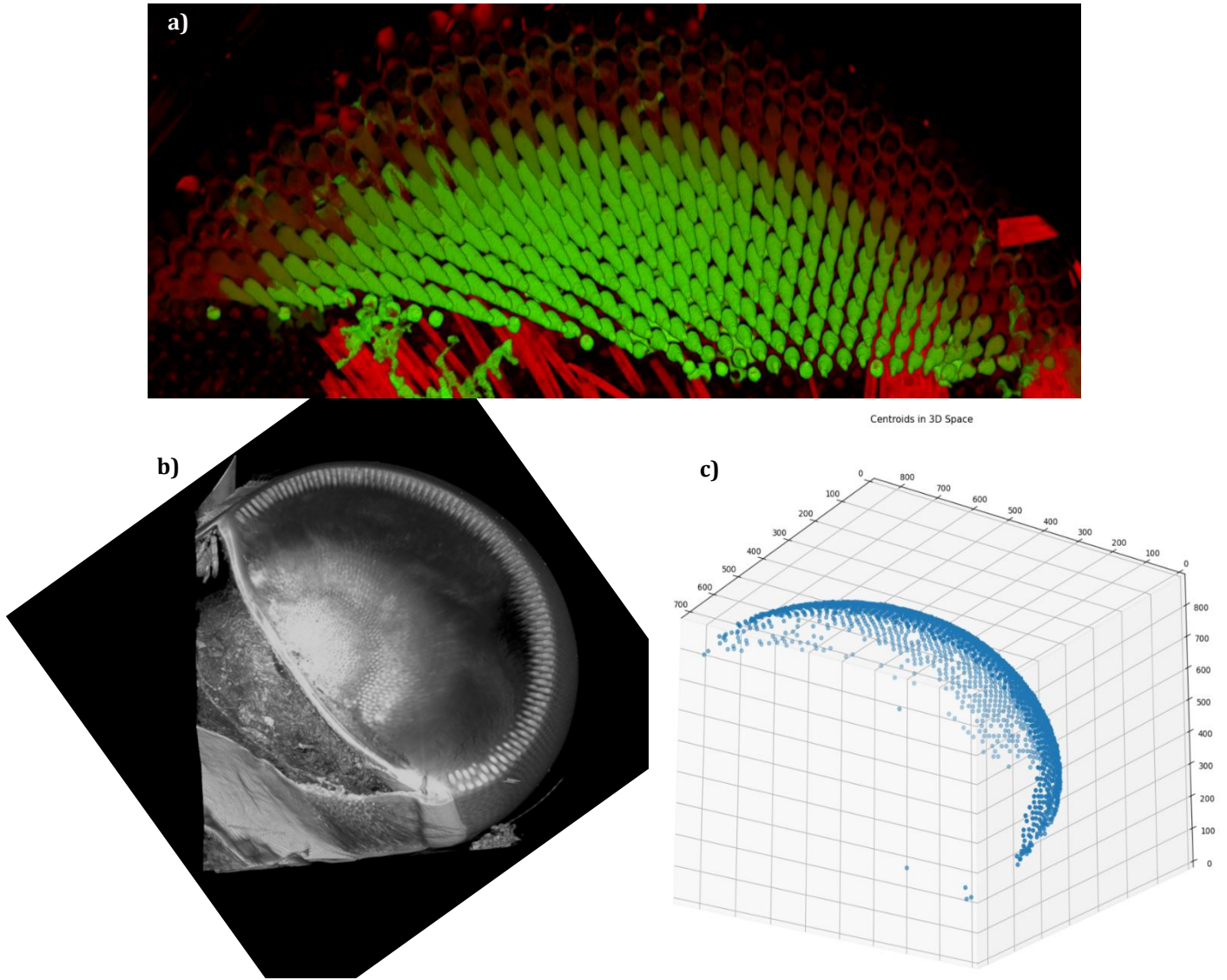
Results

This paper establishes three main results: quality of FFN segmentation, effectiveness of pipeline analysis, and biological conclusion.

Quality of FFN

The effectiveness of FFN exceeded expectations. The single model trained on a relatively small subset of data with only 32 examples was able to inference data from a broad range of ommatidial appearances (Fig. 7). Across these, FFN did an excellent job inferencing full volumes of crystalline cones (Fig. 8). Importantly, there were a marginal number of partially filled in cones and very few other artifacts of inference after cleaning. Across full eye samples, FFN was able to accurately fill in full volumes of between 1,000 and 2,000 cones per specimen (this number varied significantly for each specimen, however). FFN did an excellent job recreating the entirety of the volume of the cones and, more importantly, was able to preserve characteristic anatomical properties.

There were a few specimens that the FFN model did not generalize to, resulting in sparse and poor segmentations. These specimens were not included in this paper, and the model's failure to generalize in these is discussed later.

Pipeline Effectiveness

The effectiveness of the pipeline is entirely established in how correct the math is at determining anatomical properties of the ommatidia, both global and local. The global

Fig. 8: *Illustrations of effectiveness of FFN in inferencing ommatidia. **a)** Partial 3D rendering of the eye of a crepuscular specimen, focusing only on a section of ommatidia. **Red** shows the raw image and **Green** shows the resulting FFN inference (after cleaning). The ommatidia are almost perfectly filled in. **b)** 3D rendering of an eye from a nocturnal specimen. Ommatidia make up the ring of cones around the edge of the eye. Side of eye is truncated to allow for internal view. **c)** 3D plot of centroids of ommatidia automatically inferenced. **a)** is a different specimen than **b)** and **c)**, which are from the same specimen.*

properties are necessary to establish the relationship between ommatidia (ϕ) while the local properties establish the individual resolving power of each ommatidia (θ). Both ϕ and θ are necessary to calculate the Barlow Ratio.

To determine ϕ, the angle between ommatidia, we need to find the angle between the "directional" axes of two neighboring ommatidia (see Fig. 4). This requires an accurate characterization of this axis as well as an accurate pairing of nearest ommatidia. The use of primary

PCA serves as an equivalent to this axis and extending these axes from their centroids clearly shows a small area of focus defined (Fig. 9a). The use of scikit-learn's nearest neighbor algorithm provided a consistent and correct pairing of nearest neighbors based on centroids (Fig. 9b).

To calculate θ, the only information needed is the diameter of the base of the cone. The method used to determine diameter, which was essentially to flatten the cone by subtracting the first PCA axis from the full volume of a cone, can
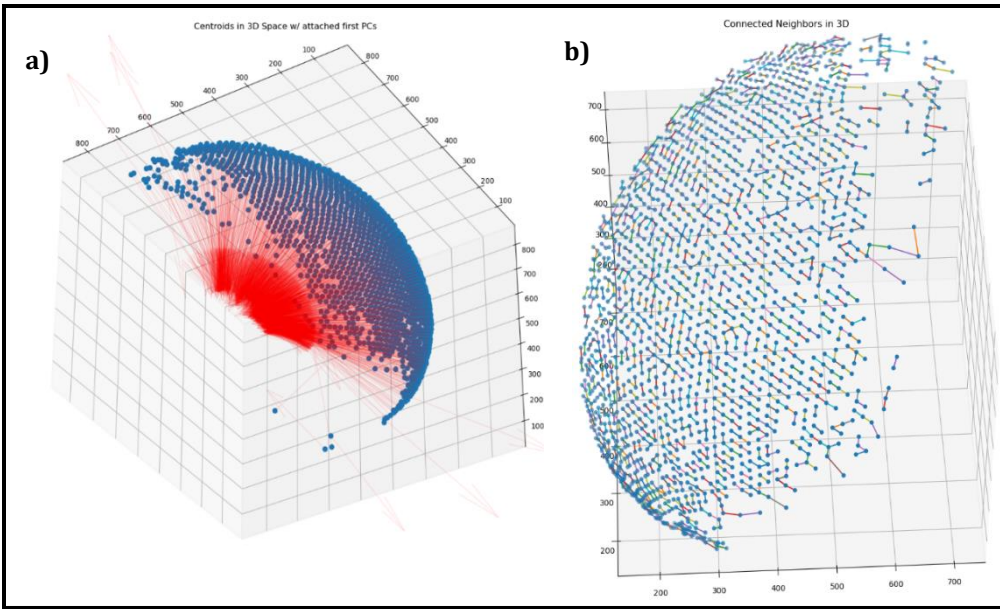
*Fig. 9: Images illustrating the accuracy of ϕ calculations using the pipeline. **a)** Centroids of inferenced ommatidia with first PCAs displayed as red arrows attached to each centroid. PCAs depict the primary axis of variance in each volume, which are equivalent to the direction of the lens-effect each ommatidia produce. **b)** Centroids of inferenced ommatidia with lines drawn between nearest neighbors.*

be trusted if the primary PCA axes are correct and that the volumes of the cones are correct. The efficacy of both is established above. To further support that the volume analysis is correct, I turn to the 'platonic' cones produced in the pipeline. There is impressive similarity in shape between cones made of the points that occur very consistently (90%+), moderately consistently (~70%) and quite inconsistently (~40%) within the crystalline cone volumes (Fig. 10). Only if the PC axes correctly represent the same properties of all the crystalline cones would the shapes be so consistent. Further, these look very similar to volumes of actual crystalline cones (Fig. 10b).

One of the diurnal specimens was removed from the data due to inconsistencies from the pipeline (discussed later).
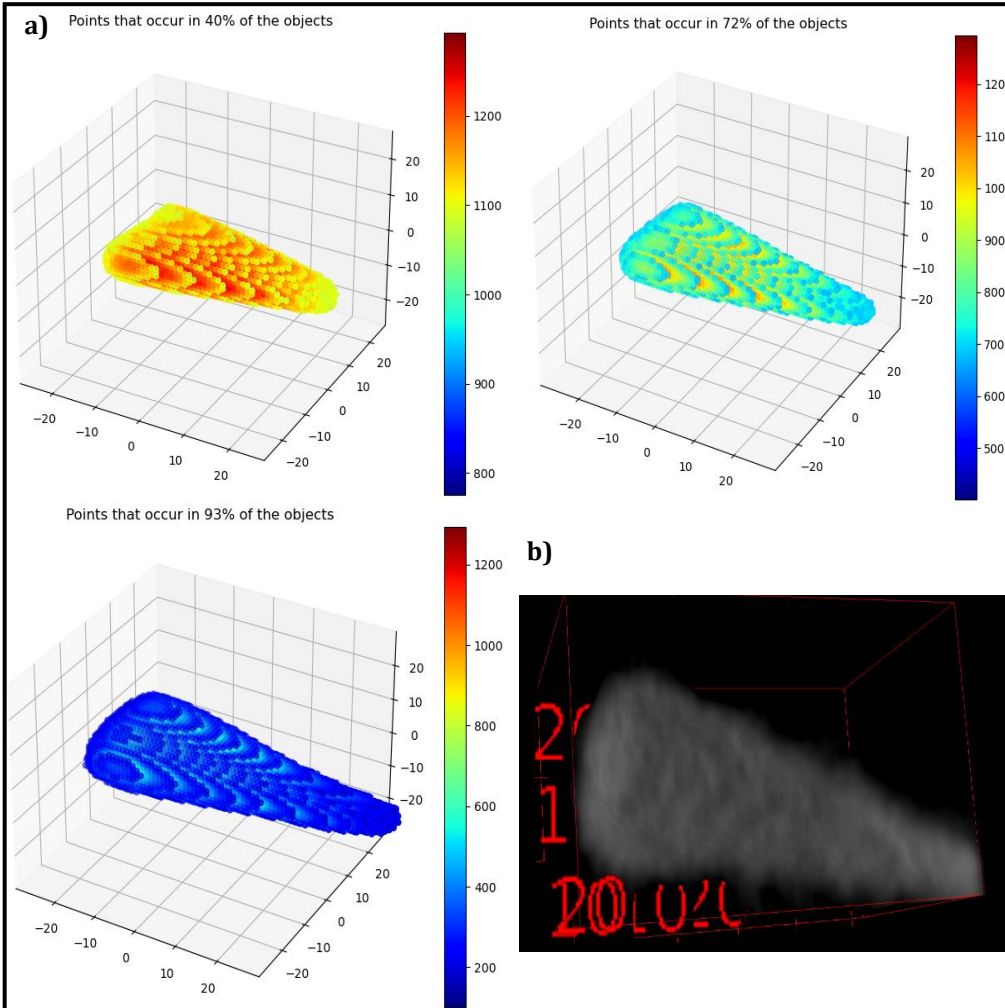

*Fig. 10: **a)** Three different 'platonic' crystalline cones generated by taking the points that occur in more than some percentage of the objects in an inferenced volume (**top left**: 93%, **top right**: 72%, **bottom left**: 40%). Ommatidia were centered and rotated in the same direction to overlap. All sample cones produced from the same data from a diurnal specimen. Colors show the frequency of the points in the data, corresponding to bar on the right of each figure. **b)** An arbitrary crystalline cone from the same specimen as the 'platonic' cones were constructed from.*

Biological Results

The pipeline collects those global and local properties of

ommatidia with the goal of enabling some rudimentary evolutionary comparisons. Primarily, it was to determine how the Barlow Ratio varies across behavioral classes. Virtually all the distributions, of all the properties measured, were significantly different from each other, but there was no observable differentiations based on behavior.

Next, the distributions were scaled down by the heights of the eye of each specimen. Interestingly, we do see that there is grouping in behaviors in ommatidia diameter and distance between ommatidia (Fig. 11c-d). The diurnal has closer cones with smaller diameters, the nocturnal have cones that are further away but far larger in diameter, while crepuscular have the farthest distance between cones and diameters in between nocturnal and diurnal.

As an aside, and for someone better equipped than I am for such analysis, I include a diagram showing the different 'platonic' cones for
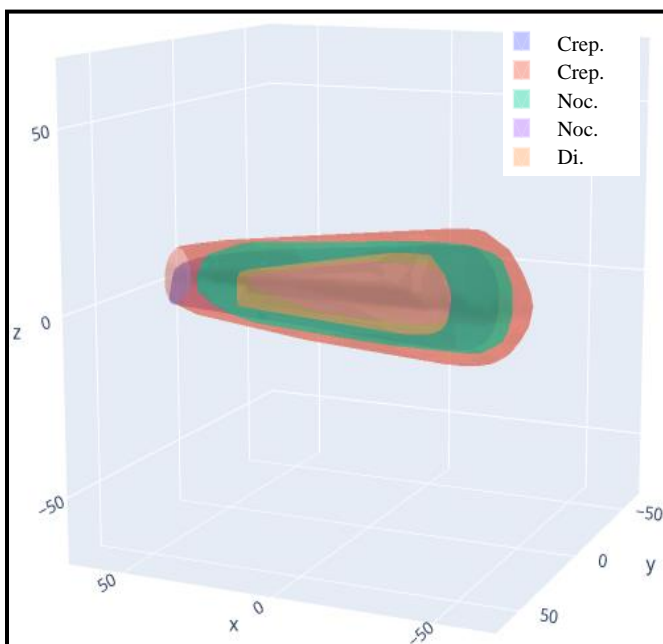

Fig. 11: Overlayed convex hulls of 'platonic' ommatidia from different specimens with different behaviors.

each specimen that were produced (Fig. 12). These show clear distinctions in volume, and some minor distinctions in their physiology, but analysis of such is beyond the scope of this paper.

Discussion

Application of FFN

FFN exceeded expectations in acquiring volumetric information of crystalline cones in a variety of eye volumes. Importantly, FFN significantly (100-1000 fold) decreases the time and manual work needed to segment these volumes. FFN did create a significant number of artifacts, but a simple cleaning script proved highly effective in removing these artifacts.

As mentioned earlier, the model I trained did not consistently work on some eye volumes. These were generally volumes that had a significant number of artifacts from the microtomography, or otherwise had crystalline cones that were not easily identifiable (even by human eye). It would likely be possible to train another FFN model to work for those volumes, as the generalizability of FFN is well established. Similarly, FFN models can be trained to collect volumetric information on any other stereotyped feature and used to collect large amounts of data for analysis.
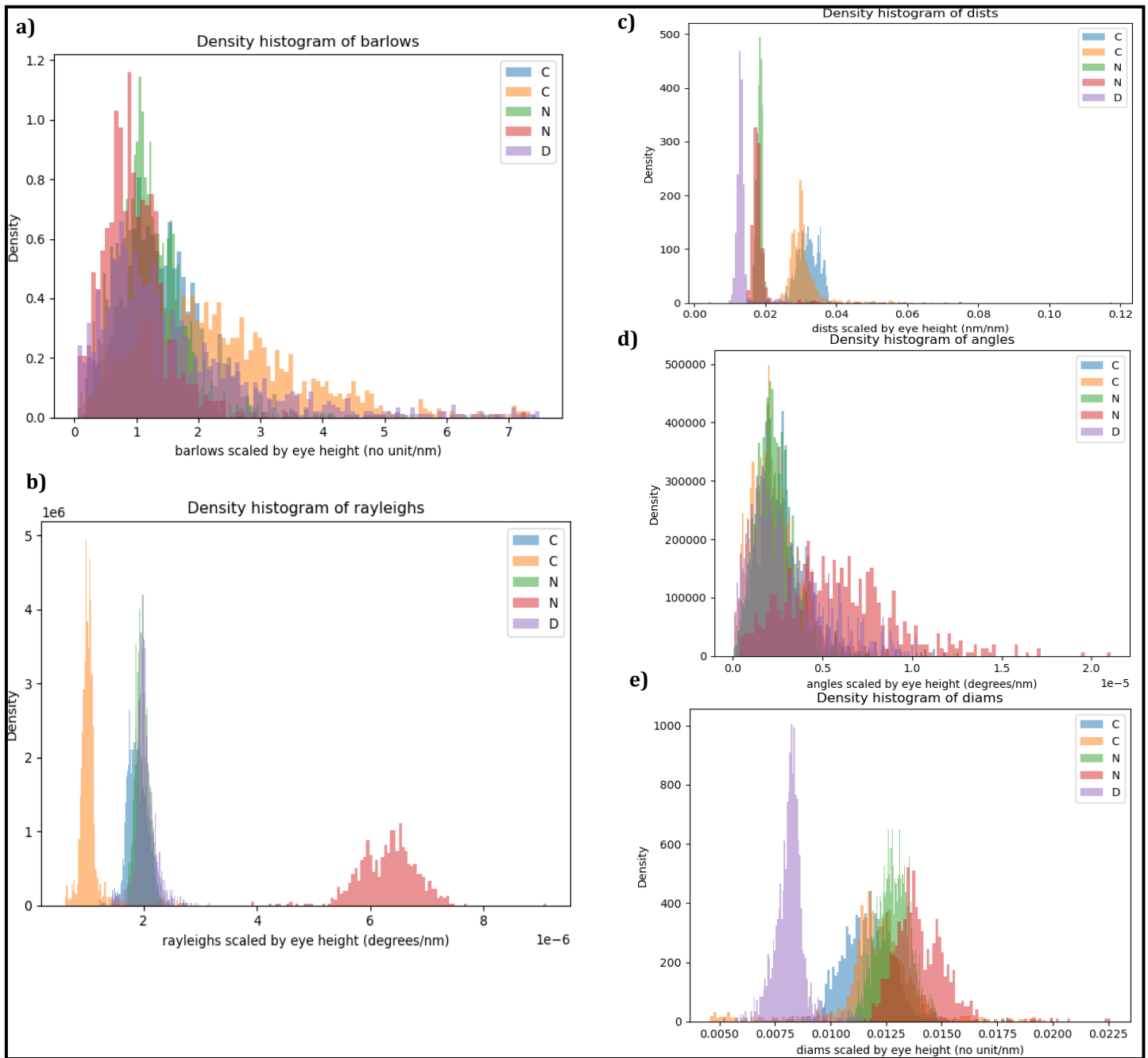
Fig. 12*: Normalized histograms of Barlow Ratio (**a**)) and influencing factors (**b**)-**e**)) across different evolutionary behaviors. **a**) Overlayed histogram of Barlow Ratios for five different samples. **b**) Overlayed histogram of angle of maximum resolving power (θ) (degrees). **c**) Overlayed histogram of distances between nearest pairs for each specimen. **d**) Overlayed histogram of interommatidial angles (φ) of each specimen. **e**) Overlayed histogram of diameters of ommatidia for each specimen. C = Crepuscular, N = Nocturnal, D = Diurnal. All the distributions are normalized relative to the height of their respective eyes. As these are all scaled down by the height of each specimen, **c**) can be thought of as an inverse to the density of crystalline cones.*

It is also worth noting that the rate of data collection was accelerated not only by FFN, but also using µXCT. Microtomography enabled very fast data collection of large volumes. Due to the relatively large size of ommatidia (compared to synapses, at least), there was no relevant information lost due to the lower resolution of µXCT as compared to traditional serial EM data collection. FFN is thus incredibly useful for the rapid collection of gross anatomical features, making it appropriate for the goals of the field. Future studies should take advantage of the data collection acceleration that microtomography and FFN allow for. Anatomical comparison of

functionally equivalent structures, be they divergent or convergent, is critical in evolutionary neuroanatomy. The collection method described here presents a way for the field to start fully utilizing the computational techniques of the 21st century.

Applicability of Pipeline

The pipeline constructed proved successful in measuring key characteristics, both global and local, of crystalline cones across multiple specimens. PCA proved to be an incredibly effective way of capturing the "direction" of each individual crystalline cone. Linear algebraic techniques proved useful in determining the diameter of the ommatidia. Pairing up nearest neighbors based on distance between centroids allowed us to determine the angle between two cones. All this analysis allowed for global measurement of Barlow Ratio and comparison of various properties across specimens with divergent behaviors.

The pipeline also allowed for the creation of a single representative crystalline cone. While analysis of these volumes is out of the scope of this project, future work plans on performing ray tracing with these volumes to simulate insect vision.

This pipeline is generally applicable for most similar volumes of ommatidia, regardless of species. The only caveat I will add is that the use of PCA implicitly assumes that the crystalline cones are truly cone-like, namely that their height is larger than their width. As such, this analysis

failed on about half of the ommatidia in one of the diurnal specimens, and so results based on this one specimen are excluded. In this scenario, the crystalline cones were very short, such that their height was similar to their width. In such a situation, the first PCA axis sometimes characterized the axis that is parallel to the base, instead of being perpendicular to the base. As a result, the PCA method did not consistently give a first axis equivalent to the 'direction' of the ommatidia. This, however, is rare, appearing in only one of the six specimens used in this paper (and only three of the fourteen full eye volumes that the lab has collected).

In general, this method of spatial characterization enables extensive comparison of compound eyes across species and behaviors. There is much about insect vision that remains undiscovered, and this pipeline, combined with the high flexibility of FFN in collecting volumetric data, represents a key first step in our ability to start understanding the evolutionary timeline of compound eyes.

Compound Eyes in Lepidoptera

At first, there did not appear to be any consistent story across the divergent behaviors – the different specimens were mixed, with no separation or clustering based on behavior (not shown). After scaling all the distributions by the respective eye heights of each specimen, however, two key patterns emerged in the behavioral grouping of distributions. First, the diameter of the cones increased as the light

amounts decreased for the active periods (Fig. 11e). Secondly, the distance between the centroids of neighboring ommatidia decreased from crepuscular (the furthest), to nocturnal, to diurnal (the shortest) (Fig. 11c). The rest of the distributions do not show any grouping by behavior, even when scaled by eye height.

This first tells us that diurnal behaviors result in the highest resolutional vision (as a function of density of ommatidia) as well as the lowest light sensitivity (as an inverse function of crystalline cone diameter). This may be a result of selective pressures in either direction – that is, a pressure to acquire higher resolution required a high density such that cones got smaller, or that a lack of necessity of high sensitivity allowed space for denser ommatidia. The data also supports a conclusion that evolutionary pressure on nocturnal species has developed far lower resolutional vision combined with much higher sensitivity compared to diurnal pressures.

More interestingly, the data supports some basic conclusions about the evolution of crepuscular insect species, such as Skippers, which are active around dusk and dawn. The evolution of this behavior must mediate between the high accuracy and low sensitivity diurnal species require (characterized by a high density of ommatidia and small diameter cones, respectively) and the low accuracy and high sensitivity that nocturnal species require (characterized by a low density of ommatidia and larger diameter cones, respectively). As such, crepuscular taxonomies have evolved a very high

density of ommatidia with moderately large diameter cones. This allows very high visual resolution paired with moderate sensitivity, which is quite useful for the moderate to low light conditions of twilight. The high resolution may also be a result of the selective pressure of predators. There are likely to be more predators present in twilight than at night, and the relative lack of light compared to daytime would make them harder to see and react to without high resolutional vision.

Even as the density of ommatidia and the diameter of crystalline cones vary with behavior, the Barlow Ratio does not seem to vary. There is a very similar ratio maintained between the angles of neighboring ommatidia and the angles of maximal resolution per each cone across both behaviors and specimens. This relative constancy is noteworthy, and its interpretations mixed. One possible interpretation is that the ratio proposed by Barlow is far too liminal for evolution – it is built on only two values and ignores much of the upstream processing that occurs in the retina and visual centers. However, it seems that Barlow was somewhat correct. The average Barlow Ratio across all the specimens was 1.28 with a standard deviation of 1.06 (this high standard deviation is due to the right-skewedness of the distribution (Fig. 13)). Barlow suggested that the Barlow Ratio ought to be between 0.4 and 1.0, and the observed average is not far from that.

Further experiments should look at more behaviors, as well as more species and specimens per behavior. Ideally, a future experiment would

compare species from the same lineage and determine if the Barlow Ratio gets closer to one (and thus more space efficient) as the species become more recent. A comparison of older and newer specimens would tell us if Barlow's predictions were ahead of evolution, and if the evolutionary trend is getting closer to his prediction.

Other studies should utilize the pipeline developed here to determine if the same narrative of crepuscular species is maintained across different orders, or if it is due to unique selective pressures that Skippers face. Comparing across behavioral types of other insects (such as ant species that rely on different forms of communication, or even between species of walking and flying ants that are otherwise similar) would also be useful to determine what selective pressures act on the evolution of ommatidia and crystalline cones. Using the ant example, ant species that rely on visual communication may require higher resolutional vision. Comparing properties of animals with compound eyes across classes, such as *Hesperidae* and the deep-sea ostracod *Macrocypridina Castanea* (Land & Nilsson, 1990), would allow comparisons of functional necessity of vision across entirely different environments. In general, the data collection and analysis pipelines discussed here show potential in further elucidation on the evolution of compound eyes.
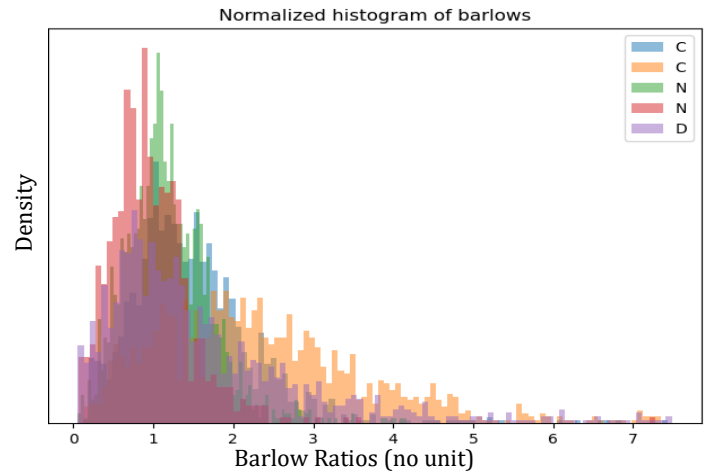

Fig. 13: *Normalized histogram of Barlow Ratios. This distribution, unlike those in **Fig. 12**, are **not** scaled by the height of the eye.*

Acknowledgements

References

Barlow, H. B. (1952). The size of ommatidia in apposition eyes. *Journal of Experimental Biology*, 667-674.

Berning, M., Boergens, K. M., & Helmstaedter, M. (2015). SegEM: Efficient Image Analysis for High-Resolution Connectomics. *Neuron*, 1193-2016.

Boergens, K. M., Berning, M., Bocklisch, T., Bräunlein, D., Drawitsch, F., Frohnhofen, J., . . . Helmstaedter, M. (2017). webKnossos: efficient online 3D data annotation for connectomics. *Nature Methods*, 691–694.

Boergens, K. M., Berning, M., Bocklish, T., Bräunlein, D., Drawitsch, F., Johannes, F., . . . Helmstaedter, M. (2017, June 12). webKnossos: efficient online 3D data annotation for connectomics. *Nature Methods*, 691–694. doi:https://doi.org/10.1038/nmeth.4331

De Carlo, F., Gürsoy, D., Marone, F., Rivers, M., Parkinson, D. Y., Khan, F., . . . Jacobsen, C. (2014 , Nov). Scientific data exchange: a schema for HDF5-based storage of raw and analyzed data. *Journal of Synchrotron Radiation*, 1224-30. doi:10.1107/S160057751401604X

Dyer, E. L., Roncal, W. G., Prasad, J. A., Fernandes, H. L., Gürsoy, D., De Andrade, V., . . . Kasthuri, N. (2017). Quantifying Mesoscale Neuroanatomy Using X-Ray Microtomography. *eNeuro*, ENEURO.0195-17.2017.

Helmstaedter, M., Briggman, K. L., Turaga, S. C., Jain, V., Seung, H. S., & Denk, W. (2013). Connectomic reconstruction of the inner plexiform layer in the mouse retina. *Nature*, 168–174.

Helmstaedter, M., Briggman, L. K., & Denk, W. (2011). High-accuracy neurite reconstruction for high-throughput neuroanatomy. *Nature Neuroscience*, 1081-1090. doi:http://www.nature.com/doifinder/10.1038/nn.2868

Hua, Y., Laserstein, P., & Helmstaedter, M. (2015). Large-volume en-bloc staining for electron microscopy-based connectomics. *Nature Communications*, 7923.

Januszewski, M., Kornfeld, J., Li, P. H., Pope, A., Blakely, T., Lindsey, L., . . . Jain, V. (2018). High-precision automated reconstruction of neurons with flood-filling networks. *Nature Methods*, 605-6012. doi:https://doi.org/10.1038/s41592-018-0049-4

Kasthuri, N., Hayworth, K., Lichtman, J., Erdman, N., & Ackerley, C. A. (2007). New Technique for Ultra-thin Serial Brain Section Imaging Using Scanning Electron Microscopy. *Microscopy and Microanalysis*, 26-27.

Land, M. F., & Nilsson, D. -E. (1990). Observations on the Compound Eyes of the Deep-Sea Ostracod Macrocypridina Castanea . *Journal of Experimental Biology*, 221-33.

Linsley, D., Junkyung, K., Berson, D., & Serre, T. (2020). Robust neural circuit reconstruction from serial electron microscopy with convolutional recurrent networks. *Unpublished manuscript*, 1-16.

MacDonald, M., Fennel, T. R., Singanamalli, A., Cruz, N. M., Yousefhussein, M., Al-Kofahi, Y., & Freedman, B. S. (2020). Improved automated segmentation of human kidney organoids using deep convolutional neural networks. *Medical Imaging 2020: Imaging Processing*, 113133B .

Peng, H., Ruan, Z., Long, F., Simpson, J. H., & Myers, E. (2010). V3D enables real-time 3D visualization and quantitative analysis of large-scale biological image data sets. *Nature Biotechnology*, 348-353.

Predegosa, F., Varoquaux, G., Gramfort, A., Michel, V., Thirion, B., Grisel, O., . . . Duchesnay, É. (2011). Scikit-learn: Machine Learning in Python. *Journal of Machine Learning Research*, 2825-2830.

Schindelin, J., Arganda-Carreras, I., Frise, E., Kaynig, V., Longair, M., Pietzsch, T., . . . Cardona, A. (2012). Fiji: an open-source platform for biological-image analysis. *Nature Methods*, 676–682.

Soltanian-Zadeh, S., Sahingur, K., Blau, S., Gong, Y., & Farsiu, S. (2019). Fast and robust active neuron segmentation in two-photon calcium imaging using spatiotemporal deep learning. *Proceedings of the National Academy of Sciences*, 116-117.

Urakubo, H., Bullmann, T., Kubota, Y., Oba, S., & Ishii, S. (2019). UNI-EM: An Environment for Deep Neural Network-Based Automated Segmentation of Neuronal Electron Microscopic Images. *Scientific Reports*, 19413.